Mean-field description of skyrmion lattice in hexagonal frustrated antiferromagnets

Oleg I. Utesov *

National Research Center "Kurchatov Institute" B.P. Konstantinov Petersburg Nuclear Physics Institute, Gatchina 188300, Russia;
Department of Physics, Saint Petersburg State University, St. Petersburg 198504, Russia;
and St. Petersburg School of Physics, Mathematics, and Computer Science, HSE University, 190008 St. Petersburg, Russia

(Received 12 October 2021; revised 17 January 2022; accepted 17 February 2022; published 28 February 2022)

A simple mean-field description of frustrated antiferromagnets on hexagonal lattices, aimed to describe the high-temperature part of the temperature-magnetic field phase diagram, is proposed. It is shown that an interplay between modulation vector symmetry, Zeeman energy, and magnetodipolar interaction leads to stabilization of the triple-Q skyrmion lattice in a certain region of the phase diagram. The corresponding analytical expressions for phase boundaries are derived. The possible relevance to the high-temperature part of the Gd_2PdSi_3 phase diagram is discussed.

DOI: 10.1103/PhysRevB.105.054435

I. INTRODUCTION

Topological phases are one of the hottest topics of contemporary solid state physics. In magnetism, individual skyrmions, skyrmion lattices (SkLs), and various other topologically nontrivial structures have been extensively studied (see, e.g., Refs. [1,2] and references therein).

In noncentrosymmetric magnets, skyrmions and SkLs were predicted theoretically in seminal papers [3,4]. Experimental observation of the SkL in the so-called A phase of MnSi [5] has stimulated a plethora of further studies on this topic. It is noteworthy that this interest is partially caused by promising technological applications (see, e.g., Refs. [6,7] and references therein).

A crucial skyrmion property relates to its nontrivial topology, which can be characterized by topological charge [8]

$$Q = \frac{1}{4\pi}\int \mathbf{n}\cdot[\partial_x\mathbf{n}\times\partial_y\mathbf{n}]dxdy, \tag{1}$$

where $\mathbf{n} = \mathbf{s}/|\mathbf{s}|$ is the unit vector along the local spin value, averaged over thermal and/or quantum fluctuations. A single skyrmion usually has $Q = \pm 1$. For a SkL the natural measure of topological charge is its density n_{Sk}, which, e.g., defines the topological contribution to the Hall resistivity, since $\rho^T \propto n_{Sk}$ [9]. In noncentrosymmetric compounds without exchange interaction frustration, where modulated spin structures are stabilized solely by Dzyaloshinskii-Moriya interaction (DMI) [10,11], the size of a magnetic unit cell is usually quite large, being of the order of the exchange constant to the DMI constant ratio (J/D) multiplied by the lattice parameter, so n_{Sk} is rather small. In contrast, in frustrated helimagnets the typical size of the magnetic unit cell is of the order of several nanometers (see Ref. [12]). This leads to large n_{Sk} and the giant topological Hall effect, which were observed in the EuPtSi [13] and Gd_2PdSi_3 [14] compounds. Interestingly, a "synergy" between DMI and frustration can lead to a drastic decrease in skyrmion size even if they are both rather weak [15].

Theoretically, stable skyrmions and SkLs in frustrated centrosymmetric helimagnets are usually ascribed to the interplay of lattice symmetry, exchange interaction, Zeeman energy, and certain kind(s) of anisotropic interactions [16–18]. For instance, in Ref. [17], multiple-Q states including the SkL were predicted at low temperatures for a triangular lattice with single-ion easy-axis anisotropy. Next, it was shown that related models with bilinear and biquadratic xxz-type exchange interactions [19] and single-ion and bond-dependent anisotropies [20] also yield rich phase diagrams in parameter space. Furthermore, recent experimental observation of the SkL in tetragonal $GdRu_2Si_2$ [21] has stimulated theoretical research, where the importance of biquadratic exchange and compass anisotropy terms has been highlighted [22,23]. A complementary high-temperature study [24] has shown that the main features of the phase diagram observed in Ref. [21] can be described within a simple model with magnetodipolar interaction and easy-axis anisotropy.

In this paper, we show the importance of dipolar forces in the phase diagram of hexagonal frustrated helimagnets, including SkL stabilization. Magnetodipolar interaction, despite being small, can play a significant role in helimagnets' properties including temperature- and magnetic-field-induced phase transitions (see, e.g., Refs. [24–32]). It is noteworthy that for magnetic ions in the spherically symmetrical $L = 0$ state (such as, e.g., Gd^{3+} in Gd_2PdSi_3 [33]) the dipolar forces are of particular importance, since the strength of other anisotropic interactions is governed by the spin-orbit coupling [34].

The rest of the paper is organized as follows. In Sec. II we present the model under consideration, discuss its main properties, and formulate the mean-field approach. In Sec. III we describe the phase transitions and phase diagram for the case of in-plane easy axes. Section IV is devoted to discussion of the relevance between the proposed approach and experimental data on the Gd_2PdSi_3 compound. In Sec. V we address the phase diagram for out-of-plane collinear easy axes. Section VI contains our conclusions. In Appendixes A–C we

*utiosov@gmail.com

provide some discussion of our treatment of magnetodipolar interaction and technical details of calculations of various phases' properties.

II. MODEL

We consider a simple model of a three-dimensional hexagonal frustrated antiferromagnet with one magnetic ion per crystallographic unit cell. The system Hamiltonian is the following:

$$\mathcal{H} = \mathcal{H}_{ex} + \mathcal{H}_d + \mathcal{H}_z, \quad \mathcal{H}_{ex} = -\frac{1}{2}\sum_{i,j} J_{ij}(\mathbf{S}_i \cdot \mathbf{S}_j),$$

$$\mathcal{H}_d = \frac{1}{2}\sum_{i,j} D_{ij}^{\alpha\beta} S_i^\alpha S_j^\beta, \quad \mathcal{H}_z = -\sum_i (\mathbf{h} \cdot \mathbf{S}_i). \tag{2}$$

Here, along with conventional symmetrical Heisenberg and Zeeman interactions [$\mathbf{h} = -g\mu_B \mathbf{H}$ is the external magnetic field in energy units (1 T $\approx$ 1.34 K)], we take into account the dipolar forces, which tensor reads

$$\mathcal{D}_{ij}^{\alpha\beta} = \omega_0 \frac{v_0}{4\pi}\left(\frac{1}{R_{ij}^3} - \frac{3R_{ij}^\alpha R_{ij}^\beta}{R_{ij}^5}\right), \tag{3}$$

where α and β denote Cartesian coordinates. The strength of the magnetodipolar interaction is governed by

$$\omega_0 = 4\pi \frac{(g\mu_B)^2}{v_0}, \tag{4}$$

which is usually about $0.1 \div 1$ K (v_0 is the unit cell volume). For instance, in Gd_2PdSi_3, one has $\omega_0 \approx 0.53$ K (here and below we use lattice parameters from Ref. [35]).

Introducing the Fourier transform

$$\mathbf{S}_j = \frac{1}{\sqrt{N}}\sum_{\mathbf{q}} \mathbf{S}_{\mathbf{q}} e^{i\mathbf{q}\mathbf{R}_j} \tag{5}$$

(where N is the total number of spins) and plugging it into the Hamiltonian (2), we get

$$\mathcal{H}_{ex} = -\frac{1}{2}\sum_{\mathbf{q}} J_{\mathbf{q}}(\mathbf{S}_{\mathbf{q}} \cdot \mathbf{S}_{-\mathbf{q}}), \tag{6}$$

$$\mathcal{H}_d = \frac{1}{2}\sum_{\mathbf{q}} \mathcal{D}_{\mathbf{q}}^{\alpha\beta} S_{\mathbf{q}}^\alpha S_{-\mathbf{q}}^\beta, \tag{7}$$

$$\mathcal{H}_z = -\sqrt{N}(\mathbf{h} \cdot \mathbf{S}_{\mathbf{0}}). \tag{8}$$

The former two terms can be combined into the bilinear part

$$\mathcal{H}_0 = -\sum_{\mathbf{q}} \mathcal{H}_{\mathbf{q}}^{\alpha\beta} S_{\mathbf{q}}^\alpha S_{-\mathbf{q}}^\beta. \tag{9}$$

The symmetrical tensor $\mathcal{H}_{\mathbf{q}}^{\alpha\beta}$ determines three eigenvalues $\lambda_1(\mathbf{q}) \geqslant \lambda_2(\mathbf{q}) \geqslant \lambda_3(\mathbf{q})$ for three mutually perpendicular eigenvectors $\mathbf{v}_1(\mathbf{q})$, $\mathbf{v}_2(\mathbf{q})$, and $\mathbf{v}_3(\mathbf{q})$. The latter can be considered as a set of principal axes for momentum-dependent biaxial anisotropy; see Appendix A 1 for a particular example and some details. Note that standard single-ion anisotropies as well as more tricky compass anisotropy [36,37] can also be included in this scheme; they simply modify $\lambda_j(\mathbf{q})$.

To describe the high-temperature part of the phase diagram, we introduce the averaged-over-thermal-fluctuations values $\langle \mathbf{S}_i \rangle \equiv \mathbf{s}_i$ and $\langle \mathbf{S}_{\mathbf{q}} \rangle \equiv \mathbf{s}_{\mathbf{q}}$. Near the ordering temperature, $|\mathbf{s}_i| \ll S$, and we expand the free energy of the mean-field approach in powers of the order parameters as follows (see, e.g., Refs. [26,30] for details):

$$\mathcal{F} = -\sum_{\mathbf{q}} \mathcal{H}_{\mathbf{q}}^{\alpha\beta} s_{\mathbf{q}}^\alpha s_{-\mathbf{q}}^\beta - \sqrt{N}\mathbf{h} \cdot \mathbf{s}_{\mathbf{0}} + AT\sum_i s_i^2 + BT\sum_i s_i^4, \tag{10}$$

where

$$A = \frac{3}{2S(S+1)}, \quad B = \frac{9[(2S+1)^4 - 1]}{20(2S)^4(S+1)^4}. \tag{11}$$

For $S = 7/2$, one has $A \approx 0.095$ and $B \approx 0.002$.

The ordering temperature of the model (10) corresponds to the largest eigenvalue $\lambda_1(\mathbf{q})$, where the system becomes unstable towards formation of magnetic structure with the corresponding modulation vector. As the dipolar interaction is typically much smaller than the frustrated exchange coupling, this maximum approximately corresponds to the momentum $\mathbf{k}$, which maximizes $J(\mathbf{q})$ (see Appendix A 2 for details). It is usually incommensurate due to the frustration, and in low-symmetry lattices either spiral [if $\lambda_1(\mathbf{k}) = \lambda_2(\mathbf{k})$] or sinusoidal spin-density wave (SDW) [for $\lambda_1(\mathbf{k}) > \lambda_2(\mathbf{k})$] ordering emerge at $T_c = \lambda_1(\mathbf{k})/A$.

For high-symmetry lattices there can be several equivalent $\mathbf{k}$, which can lead to stabilization of various so-called multiple-Q structures, and SkLs in particular (see, e.g., Ref. [24] for a discussion of the tetragonal frustrated antiferromagnet). Below, we concentrate on a case that is relevant to Gd_2PdSi_3 [14] in which there are three equivalent in-plane modulation vectors $\mathbf{k}_1 = k(0, 1, 0)$, $\mathbf{k}_2 = k(-\sqrt{3}/2, -1/2, 0)$, and $\mathbf{k}_3 = k(\sqrt{3}/2, -1/2, 0)$ with angles of 120° among them [Cartesian coordinates are used; see Fig. 1(a)]; generalization of the results to another set of in-plane vectors is straightforward.

Importantly, the dipolar tensor for in-plane $\mathbf{q}$ has quite simple properties. Basically, it favors screw helicoids. Qualitatively, it can be understood using an analogy with Bloch domain walls in ferromagnets: The spin component along the modulation vector leads to positive correction to the magnetic structure energy from dipolar interaction. In more detail, the $\mathbf{c}$ axis is the middle one for relatively small $\mathbf{q}$ and the easy one in the rest of the first Brillouin zone [see Fig. 1(b)]. Moreover, the hard axis is approximately parallel to $\mathbf{q}$ (for high-symmetry directions it is an exact feature), so the perpendicular-to-$\mathbf{q}$ direction plays the role of the easy or middle axis [for $\mathbf{k}_{1,2,3}$ we choose the corresponding vectors as follows: $\mathbf{e}_1 = (-1, 0, 0)$, $\mathbf{e}_2 = (1/2, -\sqrt{3}/2, 0)$, and $\mathbf{e}_3 = (1/2, \sqrt{3}/2, 0)$]. This axis hierarchy is crucial for the hexagonal SkL stabilization.

III. PHASE DIAGRAM: IN-PLANE EASY AXES

First, we assume that for the modulation vectors $\mathbf{k}_j$ the middle axis is $\mathbf{c}$. So, the easy axes are lying in plane with 60° angles among them; see Fig. 2. We consider the external magnetic field along the $\mathbf{c}$ axis; the corresponding eigenvalue is $\lambda_0 = (J_{\mathbf{0}} - \omega_0 \mathcal{N}_{zz})/2 \approx J_{\mathbf{0}}/2$ (where $\mathcal{N}_{zz}$ is the demagnetization tensor component [38] for ellipsoid samples). To simplify equations, we introduce "temperature" $t = \lambda_1 - AT$ ($t > 0$ in

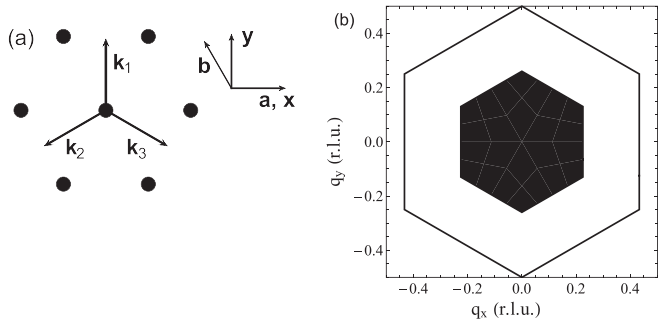

FIG. 1. (a) In the considered model, magnetic ions are arranged hexagonally in the *ab* planes, which are stacked along the **c** axis. For each incommensurate in-plane modulation vector there are at least two counterparts due to the symmetry of the system. Here, we sketch three modulation vectors observed in Gd_2PdSi_3 [14] and show the Cartesian *xyz* coordinates we use (the out-of-plane $\hat{z}$ direction is chosen along the **c** axis). (b) Due to dipolar forces, in the first Brillouin zone (large hexagon) for in-plane modulation vectors $\mathbf{q} = (q_x, q_y, 0)$ the **c** axis is the easy one outside the black hexagon, wherein it plays the role of the middle axis; the hard axis is along **q** everywhere (so, inside the black hexagon the easy axis is in plane and perpendicular to **q**). Consequently, at relatively small external magnetic fields, screw helicoids are energetically favorable. Furthermore, we show that in a large part of the phase diagram the triple-Q structure is stable.

magnetically ordered phases) and parameters $\Lambda = \lambda_1 - \lambda_2$, $\Lambda' = \lambda_1 - \lambda_3 > \Lambda$, and $\Lambda_0 = \lambda_1 - \lambda_0$. Finally, it is sufficient to substitute BT with $b = BT_c$ in Eq. (10).

Similarly to Ref. [24], we restrict our analysis to a particular set of magnetic structures. We also neglect possible small variations of the modulation vectors in phases with a multicomponent order parameter, which can appear due to the dipolar tensor eigenvalues' momentum dependence. Details of the calculations are mostly presented in Appendix B.

(i) The first structure we discuss is the simple SDW (herein referred to as 1S) with the spin ordering

$$\mathbf{s}_i = s\mathbf{e}_1 \cos \mathbf{k}_1\mathbf{R}_i + m\hat{z}, \tag{12}$$

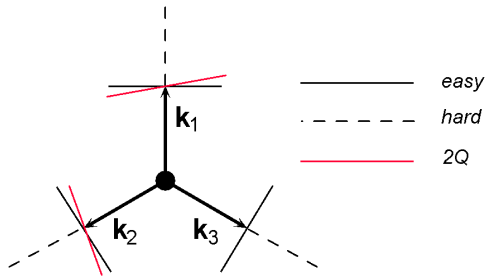

FIG. 2. Illustration for the case of in-plane easy axes considered in Sec. III. The particular orientation of easy and hard axes is the effect of dipolar forces (see Appendix A 1 for details). When considering double-modulated structures (2S and 2Q) with, e.g., $\mathbf{k}_1$ and $\mathbf{k}_2$, the choice of two easy axes for in-plane modulated spin components leads to an increase in their free energy making it larger than that of the 1S and 1Q phases. In contrast, when the in-plane components are polarized along the red axes, 2S and 2Q can become stable in some part of the phase diagram (see Sec. IV).

where one can choose any $\mathbf{k}_j$ and arbitrary phase of cosine. The corresponding free energy per one spin reads

$$\mathcal{F}_{1S} = -\frac{t}{2}s^2 - hm - (t-\Lambda_0)m^2 + b\left(m^4 + m^2s^2 + \frac{3}{8}s^4\right). \tag{13}$$

(ii) The second structure is the helicoid with spins rotating in the easy plane perpendicular to **k** (1Q structure). Taking, e.g., $\mathbf{k}_1$, we have

$$\mathbf{s}_i = s\mathbf{e}_1 \cos \mathbf{k}_1\mathbf{R}_i + p\hat{z} \sin \mathbf{k}_1\mathbf{R}_i + m\hat{z}. \tag{14}$$

Here, $sp > 0$ corresponds to the right spiral, and $sp < 0$ corresponds to the left one; the common phase of sine and cosine functions can be chosen arbitrarily. The free energy is given by

$$\mathcal{F}_{1Q} = -\frac{t}{2}s^2 - \frac{t-\Lambda}{2}p^2 - hm - (t-\Lambda_0)m^2 + b\left[m^4 + m^2(s^2+3p^2) + \frac{3s^4+2s^2p^2+3p^4}{8}\right]. \tag{15}$$

(iii) The third structure is the conical cycloid with spins rotating in the *ab* plane, perpendicular to the magnetic field (XY structure):

$$\mathbf{s}_i = s\mathbf{e}_1 \cos \mathbf{k}_1\mathbf{R}_i + p\hat{z} \times \mathbf{e}_1 \sin \mathbf{k}_1\mathbf{R}_i + m\hat{z}. \tag{16}$$

The corresponding free energy per one spin reads

$$\mathcal{F}_{XY} = -\frac{t}{2}s^2 - \frac{t-\Lambda'}{2}p^2 - hm - (t-\Lambda_0)m^2 + b\left[m^4 + m^2(s^2+p^2) + \frac{3s^4+2s^2p^2+3p^4}{8}\right]. \tag{17}$$

Important differences compared with Eq. (15) are the following: Eq. (17) contains Λ' instead of Λ and bm^2p^2 instead of $3bm^2p^2$, so at low magnetic fields the 1Q structure is preferable, but at stronger fields $\mathcal{F}_{XY}$ becomes smaller.

These single-modulated spin structures [structures (i)–(iii)] are depicted in Fig. 3.

(iv) The fourth structure is the superposition of three screw helicoids (3Q) [Fig. 4]. In general, this spin ordering reads

$$\mathbf{s}_i = \sum_{j=1,2,3} [s_j\mathbf{e}_j \cos(\mathbf{k}_j\mathbf{R}_i + \varphi_j) + p_j\hat{z} \sin(\mathbf{k}_j\mathbf{R}_i + \varphi_j)] + m\hat{z}. \tag{18}$$

However, a minimal free energy is achieved only if [39] [see Eq. (B10)]

$$s_1 = s_2 = s_3 = s/\sqrt{3},$$
$$p_1 = p_2 = p_3 = p/\sqrt{3},$$
$$\varphi_1 + \varphi_2 + \varphi_3 = 2\pi n + \mathrm{sgn}(p)\pi/2. \tag{19}$$

Note that the chiralities of all three helicoids are the same. The corresponding free energy is given by

$$\mathcal{F}_{3Q} = -\frac{t}{2}s^2 - \frac{t-\Lambda}{2}p^2 - hm - (t-\Lambda_0)m^2 + b\left[m^4 + m^2(s^2+3p^2) + \frac{9s^4+10s^2p^2+15p^4}{24} - \frac{mp(2p^2+s^2)}{\sqrt{3}}\right]. \tag{20}$$

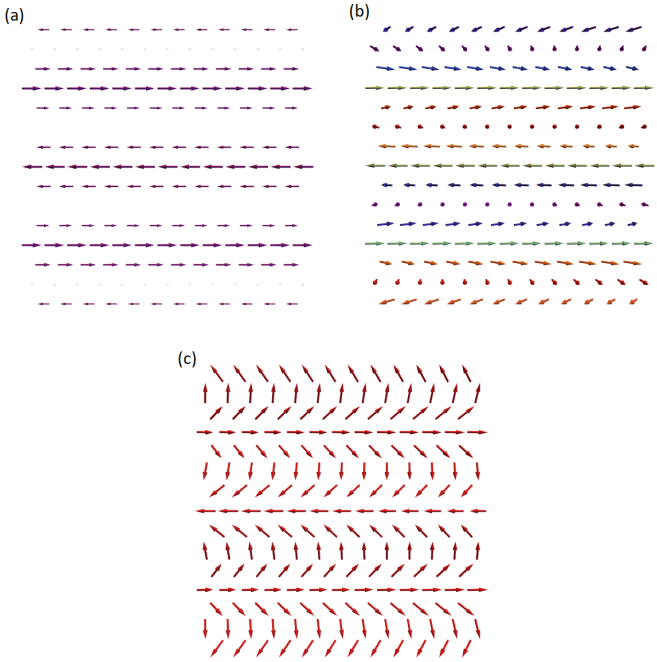

FIG. 3. Single-modulated spin structures considered in the proposed theory. Modulation vector $\mathbf{k}_1$ is taken for all the structures. (a) Simple spin-density wave ($1S$) with collinear spin ordering. (b) Elliptical helicoid ($1Q$) with spins rotating in plane perpendicular to the modulation vector [red spins are "up" and violet ones are "down" along the direction perpendicular to the figure plane (ab)]. (c) Conical cycloid (XY) where spins rotate in the ab plane and there is a constant magnetization component along the external field.

The last term here is crucial. Note that if all $p_j = 0$ in Eq. (18), the corresponding magnetic structure is a triple SDW, or $3S$. Moreover, its free energy is the same as that of the simple $1S$ structure [40]. However, it is evident from Eq. (20) that even at infinitesimal h, when nonzero m appears, $3S$ is unstable towards transition to $3Q$. So, for in-plane easy axes, $\mathcal{F}_{3Q}$ is always smaller than $\mathcal{F}_{1S}$ and $\mathcal{F}_{3S}$.

(v) The fifth structure is the superposition of two SDWs ($2S$) and two screw helicoids ($2Q$). These magnetic structures

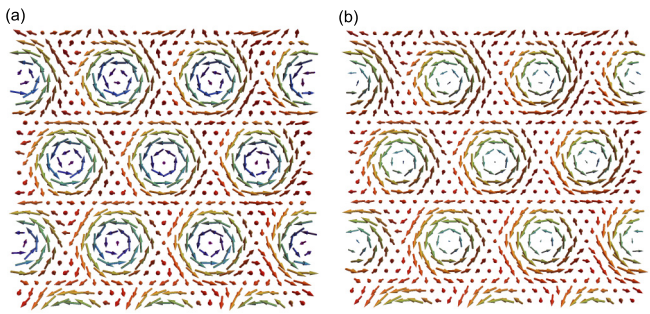

FIG. 4. The $3Q$ phase, which is a superposition of three homochiral (left or right) helicoids and a uniform magnetization component, can be either topologically nontrivial at moderate magnetic fields (a), where spins wrap around a sphere once per skyrmion, or trivial (b) at fields close to the saturation one (see Fig. 6). Here, $\mathbf{h} \uparrow\uparrow \hat{z}$, red spins are "up" ($s_z > 0$), and violet spins are "down" ($s_z < 0$).

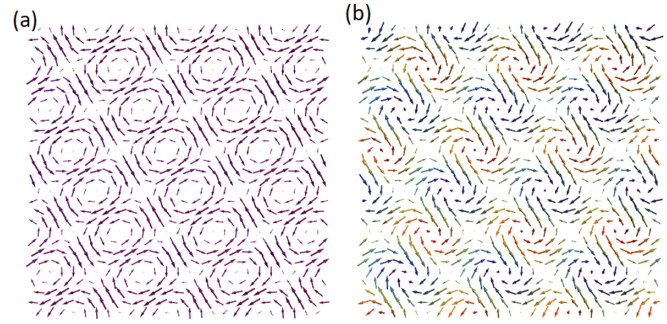

FIG. 5. Illustration of double-modulated spin structures with $\mathbf{k}_1$ and $\mathbf{k}_2$ modulation vectors at zero magnetic field. (a) Double spin-density wave ($2S$) which is a vortical structure. (b) Superposition of two elliptical helicoids ($2Q$): meron-antimeron lattice with average $n_{Sk} = 0$ [41]. However, at finite magnetic field, nonzero spins emerge in the nodes (points where $\mathbf{s}_i = \mathbf{0}$) of this structure, and the whole lattice become topologically nontrivial (see, e.g., a similar discussion in Ref. [24]).

were shown to be stable in tetragonal frustrated antiferromagnets with dipolar forces in Ref. [24]. However, in that study the in-plane spin components with different modulation vectors were oriented in perpendicular directions, in-plane easy axes. Here, if one considers the $2Q$ spin structure given by Eq. (18) with, e.g., modulation vectors $\mathbf{k}_1, \mathbf{k}_2$ and $s_1 = s_2 = s$, $s_3 = 0$ and $p_1 = p_2 = p$, $p_3 = 0$, it is evident from Eq. (B10) that this structure has no advantages in comparison with $1Q$ and $3Q$ because the last term of Eq. (B10) in this case is always zero.

So, in order to have a stable double-modulated phase, we choose two modulation vectors $\mathbf{k}_i$ and two mutually perpendicular directions for in-plane spin components, which minimize the anisotropy energy (they are rotated by $\phi = 15^\circ = \pi/12$ from the easy axes; see Fig. 2). For instance, after taking $\mathbf{k}_1$ and $\mathbf{k}_2$ we have

$$\mathbf{s}_i = \sum_{j=1,2} [s_j \mathbf{e}'_j \cos(\mathbf{k}_j \mathbf{R}_i + \varphi_j) + p_j \hat{z} \sin(\mathbf{k}_j \mathbf{R}_i + \varphi_j)] + m\hat{z}, \tag{21}$$

where directions $\mathbf{e}'_j$ are shown by red color in Fig. 2. The corresponding $2S$ structure with $p_j = m = 0$ and $2Q$ structure with $m = 0$ are shown in Fig. 5. In order to describe their free energy, one should use the eigen-numbers $\tilde{\lambda}_1 = \lambda_1 \cos^2\phi + \lambda_3 \sin^2\phi$ and λ_2. It is convenient to introduce $\delta\Lambda = \lambda_1 - \tilde{\lambda}_1$. For the $2Q$ structure with equal order parameters $s_1 = s_2 = s/\sqrt{2}$ and $p_1 = p_2 = p/\sqrt{2}$ (other structures have larger free energy) we have

$$\mathcal{F}_{2Q} = -\frac{t - \delta\Lambda}{2} s^2 - \frac{t - \Lambda}{2} p^2 - hm - (t - \Lambda_0) m^2 + b\left[m^4 + m^2(s^2 + 3p^2) + \frac{5s^4 + 6s^2p^2 + 9p^4}{16}\right]. \tag{22}$$

The $2S$ free-energy function is a particular case of this equation with $p = 0$.

Competition of these phases with $1S$ and $1Q$ was studied in detail in Ref. [24] for $\delta\lambda = 0$, with the main result that at fixed moderate magnetic field, a paramagnetic (PM)

$\leftrightarrow 2S \leftrightarrow 2Q \leftrightarrow 1Q$ sequence of phase transitions appears. However, nonzero $\delta\Lambda$ makes $\mathcal{F}_{2Q}$ (and $\mathcal{F}_{2S}$) larger; the double-modulated structures' region of stability in the phase diagram can only be observed at $\delta\Lambda \ll \Lambda$, and it collapses at $\delta\Lambda \lesssim \Lambda$ (see Appendix B). So, in this section, we will consider the phase diagram topology without these phases and postpone the corresponding discussion to Sec. IV.

We note that all the phases above have longitudinal spin modulations, which are typical for helimagnets near the ordering temperature [42].

For analytical treatment of various spin structures' free energies we neglect derivatives of terms with the fourth power of order parameters in equation $\partial\mathcal{F}/\partial m = 0$, assuming that the system is not close to ferromagnetic instability near T_c. So, the magnetization simply reads

$$m(t,h) = \chi(T)h = \frac{h}{2(\Lambda_0 - t)}. \tag{23}$$

Furthermore, usually $\Lambda_0 \gg \Lambda, \Lambda'$, and it is sufficient to put $\chi \equiv \chi(T_c) = 1/2\Lambda_0$ instead of $\chi(T)$. Under this assumption, it is fruitful to use in calculations renormalized by terms $\propto m^2$ parameters t and Λ:

$$t_h = t - 2b(\chi h)^2, \tag{24}$$

$$\Lambda_h = \Lambda + 4b(\chi h)^2. \tag{25}$$

Then, it is easy to show that both $1S$ and $3Q$ phases require $t_h > 0 \Leftrightarrow t > 2b(\chi h)^2$. This determines the boundary between $3Q$ and the paramagnetic (or field-polarized) phase, PM.

If we opt for not taking into account $3Q$ (and other multiple-Q structures), a simple phase diagram (shown in Fig. 12 in Appendix B) can be obtained. The important scales here are determined by the coordinates of the triple point (where $1S$, $1Q$, and XY are in equilibrium), namely, the spiral plane flop field

$$h_{SF} = \sqrt{\frac{\Lambda' - \Lambda}{4b\chi^2}} \tag{26}$$

and the "temperature"

$$t_{\mathrm{Tr}} = 2\Lambda' - \Lambda/2. \tag{27}$$

However, $3Q$ has lower energy than $1S$, and it pushes the XY phase further away to t substantially larger than t_{Tr}. Moreover, below we show that for realistic parameters of Gd_2PdSi_3 the XY phase does not appear at all in the range of mean-field approach validity. So, the resulting phase diagram consists of $1Q$ and $3Q$ phases. The boundary between them is approximately given by

$$t_{1Q-3Q}(h) \approx \tfrac{3}{2}\Lambda + 45b(\chi h)^2. \tag{28}$$

Importantly, inside the $3Q$ phase stability domain there exists a curve dividing topologically trivial and nontrivial parts. We show these two spin structures in Fig. 4. For nontrivial structure topology with $n_{Sk} = \pm 1$ (the sign here depends on the chirality of the helicoid constituents), the spin should be able to point oppositely to the external field and magnetization. For the spin structure given by Eq. (18) under conditions (19) (and positive m) the minimal value of the spin z component is $m - \sqrt{3}p$. So, upon m growth the $3Q$ structure remains topologically nontrivial until $\sqrt{3}p > m$. When m becomes larger than $\sqrt{3}p$, the skyrmions' cores disappear, and the z component of all spins becomes positive. The spin structure in this case is kind of vortical, but with a small modulated spin component along the z axis. In our approximation this boundary can be found exactly as

$$t_{\mathrm{SkL}}(h) = \tfrac{9}{10}\Lambda + \tfrac{203}{45}b(\chi h)^2 \approx 0.9\Lambda + 4.5b(\chi h)^2. \tag{29}$$

At $t < t_{\mathrm{SkL}}$ (at larger T) the $3Q$ structure is topologically trivial with $n_{Sk} = 0$. Note that in our approach, $t_{\mathrm{SkL}}(h)$ does not have the physical meaning of a phase transition temperature. Nevertheless, one can expect some anomalies due to possible effects of topology on other, e.g., electronic, degrees of freedom. Moreover, our theory averages over thermal fluctuations, and the picture with discontinuously changing topological charge is valid only in this approach. In reality, one can expect that, e.g., at $t \lesssim t_{\mathrm{SkL}}(h)$, spin configurations in magnetic unit cells will be topologically nontrivial with some probability, and vice versa, for $t \gtrsim t_{\mathrm{SkL}}(h)$ in the $3Q$ SkL phase, thermal fluctuations will destroy some skyrmions. The latter results in the diminishing of the n_{Sk} at higher temperatures, which is always observed experimentally (see, e.g., Ref. [14]).

We first apply our theory to Gd_2PdSi_3 as is. The parameters can be estimated using the ordering temperature $T_N \approx 22$ K and the saturation field $H_S \approx 9$ T [43,44]. The former quantity determines $J_{\mathbf{k}}$ for $k = 0.14$ [14] (in reciprocal lattice units, r.l.u.), whereas the second one can be used to estimate $J_{\mathbf{0}}$, since $h_S \approx S(J_{\mathbf{k}} - J_{\mathbf{0}})$ in frustrated helimagnets (see, e.g., Refs. [32,45]). Dipolar tensor components were calculated using their representation in the form of fast-converging sums (see, e.g., Ref. [46]). As a result we get (all values are in kelvins)

$$\begin{aligned} &J_{\mathbf{k}} \approx 4.00, \quad J_{\mathbf{0}} \approx 0.56, \quad \Lambda \approx 0.02, \\ &\Lambda' \approx 0.26, \quad \Lambda_0 \approx 1.72. \end{aligned} \tag{30}$$

Using this set of parameters, we obtain the phase diagram shown in Fig. 6. Note that the $2S$ and $2Q$ phases do not appear in the phase diagram, the reason being that for parameters (30), $\delta\Lambda \approx \Lambda$, which is a big disadvantage for them with regard to anisotropic energy.

The type of phase diagram shown in Fig. 6 is quite general (in a qualitative sense) for the model with in-plane easy axes. Nevertheless, by varying the parameters, the XY phase can appear in the approach validity region. We illustrate this statement by manually setting $\Lambda' = 0.05$ in Eq. (30), which results in the phase diagram shown in Fig. 7 with observable regions of the conical phase. We would like to point out that in this case, $T_{\mathrm{Tr}} \approx 21$ K but XY emerges only at $T \approx 18$ K due to the competition with $3Q$. Note also the appearance of the $2S$ phase in a small part of the phase diagram due to the much smaller $\delta\Lambda \approx 0.003$ in this case.

IV. DOUBLE-MODULATED PHASES AND POSSIBLE RELEVANCE TO Gd_2PdSi_3 PHASE DIAGRAM

We see that the phase diagram obtained in the previous section is substantially different from the one discussed in the literature for the Gd_2PdSi_3 compound. Although it also

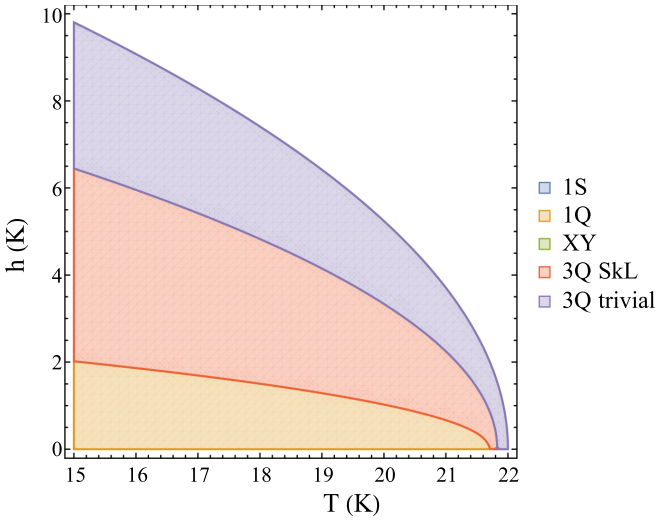

FIG. 6. High-temperature part of the phase diagram for the considered model (see Fig. 1). Parameters (30) are used. As usual for dipolar-forces-induced anisotropy, the simple SDW (1S) and conical helicoid (XY) (see Fig. 12) do not appear in this region of the phase diagram. They are substituted by the 3Q phase in its topologically trivial and nontrivial forms (see text). It is pertinent to provide some order parameter values. For instance, at $T = 19$ K and $h = 0$ K (1Q phase), $s \approx 1.9$, $p \approx 1.8$, and $m = 0$, whereas at $T = 19$ K and $h = 4$ K (3Q SkL phase) $s \approx 1.9$, $p \approx 0.8$, and $m \approx 1.2$; so the average spin value is not close to saturation ($S = 7/2$), and the theory still has a small parameter $s_i^2/S^2 \approx 1/4$.

contains the 3Q SkL stability region, there are several major issues in comparison with the data of Refs. [14,43,44]. First, the low-h–low-T phase in Fig. 6 (1Q) does not have scalar spin chirality, whereas scalar spin chirality was observed experimentally at nonzero h [14]. Second, in our approach, the 3Q SkL can be found at zero h, while experimentally this is not the case [14,43]. The third minor issue is the modulated z

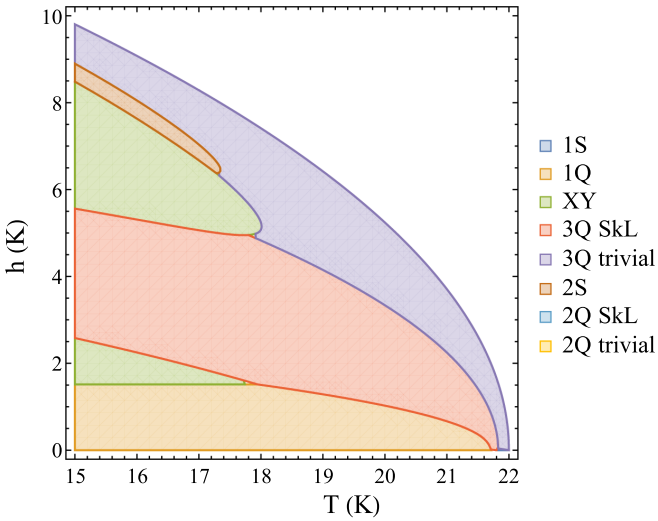

FIG. 7. If one makes the value of parameter Λ' in set (30) smaller, then the XY phase appears on the phase diagram (cf. Fig. 6). However, the 3Q SkL phase is still the ground state in a large part of the phase diagram.

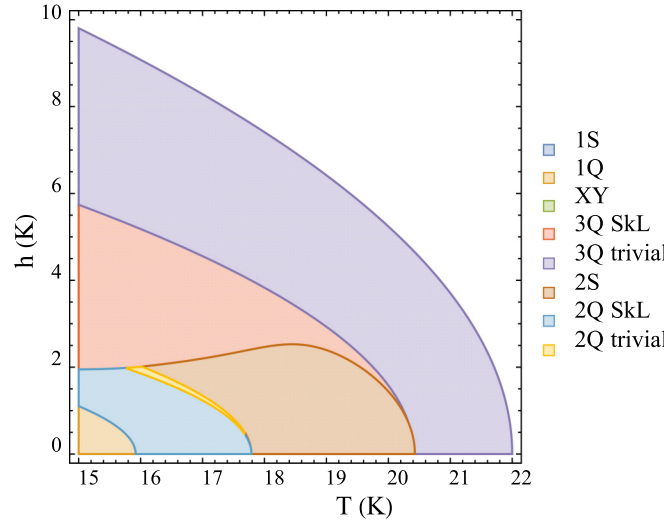

FIG. 8. Phase diagram obtained within the proposed approach at $\delta\Lambda \ll \Lambda$, where the 2$S$ and 2Q phases can appear at low h (cf. Fig. 6). It can be relevant to Gd_2PdSi_3. Note that the 1Q phase appears only in the region when the small-s_i approach fails.

component of spin in the 3Q trivial phase, which is, however, small at $T \lesssim T_N$. So, the 3Q trivial phase looks almost like the vortex phase proposed in Ref. [26] near its boundary with the PM phase. Moreover, at smaller T near the fully polarized phase the constant spin component m becomes $\sim S$, and the most likely scenario (which cannot be described in our high-temperature approach) is stabilization of the conventional single-modulated fan structures or, possibly, their multiple-Q counterparts [20].

Regarding the low-h part of the phase diagram, we would like to note that the triangular meron-antimeron lattice, which is a 3Q structure with $\varphi_1 + \varphi_2 + \varphi_3 = \pi n$, in our high-temperature approach always has larger free energy than the simple 1Q helicoid [see Eq. (B10), where the last term is zero in this case]. We can make the conclusion that in the small-s expansion there are no reasons for triangular meron-antimeron lattice stabilization. However, we note that this structure can be stabilized in systems with a more complicated Hamiltonian that includes biquadratic exchange and Dzyaloshinskii-Moriya interaction [47].

Since the model under consideration lacks DMI, we believe that the 2Q structure shown in Fig. 5(b) can be considered as a candidate for the incommensurate-1 (IC-1) phase observed experimentally (see Ref. [14]). It is a topologically trivial (on average) meron-antimeron lattice [41] at $h = 0$, but nonzero magnetic field induces the average topological charge. In order to observe double-modulated spin structures, we modify parameters (30) to have $\delta\Lambda \ll \Lambda$ (under the condition that the **c** axis remains the middle one). Playing with the parameters, we observe the phase diagram shown in Fig. 8. Here, additional single-ion easy-plane anisotropy with constant 0.15 K along with anisotropic exchange (bond-dependent anisotropy) making λ_3 larger by $\approx$0.07 K is taken into account. In Fig. 8 one can see several important features: (i) The 3Q SkL phase is stable only at finite magnetic fields; (ii) there is a vortexlike double-modulated structure 2S, which can possibly describe

the intermediate IC-3 phase observed in Ref. [44]; (iii) there is a $2Q$ phase (note that it can be topological and trivial at $h > 0$ as in Ref. [24]), which possibly represents the IC-1 phase discussed above; and (iv) there is a $1Q$ structure, however, only in the region where our approach is unreliable.

So, we make the conclusion that the developed framework arguably allows one to describe the high-temperature part of the Gd_2PdSi_3 phase diagram. At the same time, we cannot exclude the possibility that considering other interactions (e.g., biquadratic exchange) could be important.

Finally, we note that in-plane momentum-dependent anisotropy (in the form of dipolar forces or anisotropic exchange) should be important for low-temperature depinned phase [43] description. Moreover, the spiral plane anisotropy for depinned $\mathbf{q}$ under in-plane $\mathbf{h}$ supports the idea of the fan-phase stabilization; the corresponding theoretical framework was developed in Ref. [32].

V. PHASE DIAGRAM: EASY AXIS ALONG c

According to Fig. 1 there is a possibility to have collinear easy axes along $\mathbf{c}$ for all three $\mathbf{k}_j$ solely due to dipolar interaction. However, this requires rather large k. At the same time, standard single-ion easy-axis anisotropy can also change the axes' hierarchy (its constant should be subtracted from the $\mathcal{H}_{\mathbf{q}}^{\alpha\beta}$ in-plane eigenvectors' eigenvalues and added to the ones corresponding to the $\mathbf{c}$ axis). In both cases we arrive at a substantially different phase diagram, which is discussed below.

First, we point out important differences compared with the previous case: (i) The modulated component of $1S$ is now along $\hat{z}$; (ii) for free energies of the $1Q$ and $3Q$ phases, $t - \Lambda$ is multiplied on s^2, not on p^2 as previously; and (iii) in a magnetic field the following counterparts of Eqs. (24) and (25) should be used:

$$t_h = t - 6b(\chi h)^2, \tag{31}$$

$$\Lambda_h = \Lambda - 4b(\chi h)^2. \tag{32}$$

Importantly, here the in-plane s component of $3Q$ and $1Q$ structures appears only at $t > 3\Lambda/2$ (see Appendix C for details). At lower t the $1S$ phase competes with the bubble phase we call here $3P$, which is the superposition of three collinear spin-density waves [48]; see Fig. 9. If we fix certain $t < 3\Lambda/2$ and increase h starting from $h = 0$, we have the sequence of phase transitions $1S \to 3P \to$ PM. Both transitions are of the first order.

At $t > 3\Lambda/2$ (lower T), this sequence transforms into $1Q \to 3Q \to$ PM. The former transition is always a first-order one; however, the latter can be either continuous or discontinuous. The reason is that in a small vicinity of $t = 3\Lambda/2$ the $3Q$ phase is topologically nontrivial in the whole range of fields till the PM phase becomes the ground state. For yet larger t, before the PM phase appears, the $3Q$ phase becomes topologically trivial (either smoothly or discontinuously; see Appendix C).

As a result, using parameter set (30) (note that if we keep the same $\mathbf{k}_j$ as in the previous sections of this paper, it implies single-ion easy-axis anisotropy with the constant equal to 2Λ, which makes $\mathbf{c}$ the easy direction), we obtain the phase diagram shown in Fig. 10. Note that double-modulated spin structures $2S$ and $2Q$ do not appear in this case. For the out-of-plane easy axis they were previously shown to be stabilized in the moderate-h part of the phase diagram (see Fig. 5 of Ref. [24]); however, here we also have $\delta\Lambda \sim \Lambda > 0$, and they "lose the competition" with the $3Q$ structures.

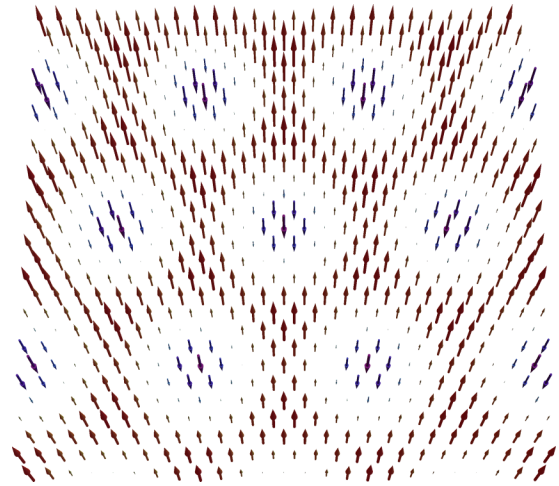

FIG. 9. When the easy axes are along $\mathbf{c}$, a peculiar bubblelike $3P$ phase can be stable near T_c in the external field. It consists of three collinear spin-density waves.

The boundary between $1S$ ($1Q$) and $3P$ ($3Q$) is approximately given by

$$t_{1S-3P} \approx 40b(\chi h)^2, \tag{33}$$

whereas the boundary between $3P$ and PM reads

$$t_{3P-\mathrm{PM}} = \tfrac{74}{15}b(\chi h)^2. \tag{34}$$

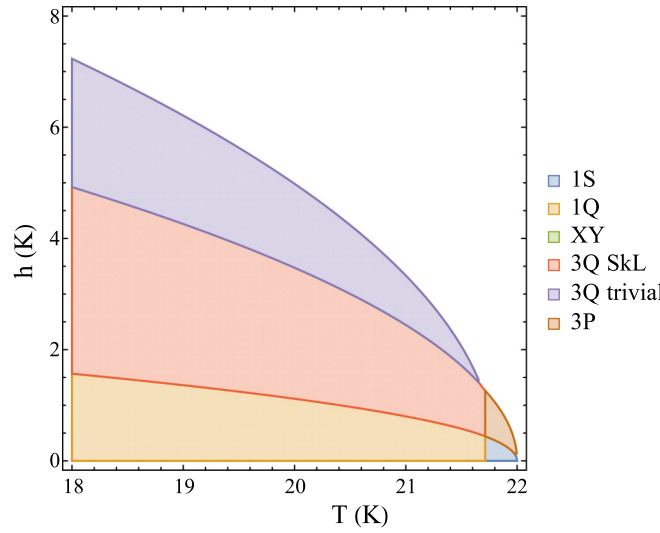

FIG. 10. Same as Fig. 6, but for the system with collinear easy axes along $\mathbf{c}$. Parameters (30) are used. Note that the superposition of three collinear spin-density waves, the $3P$ phase (see Fig. 9), appears. Typical values of the order parameters here are the following: At $T = 20$ K and $h = 0$ K ($1Q$ phase), $s \approx 1.4$, $p \approx 1.5$, and $m = 0$, whereas at $T = 20$ K and $h = 4$ K ($3Q$ SkL phase) $s \approx 1.4$, $p \approx 1.0$, and $m \approx 0.9$; so $s_i^2/S^2 \approx 1/5$.

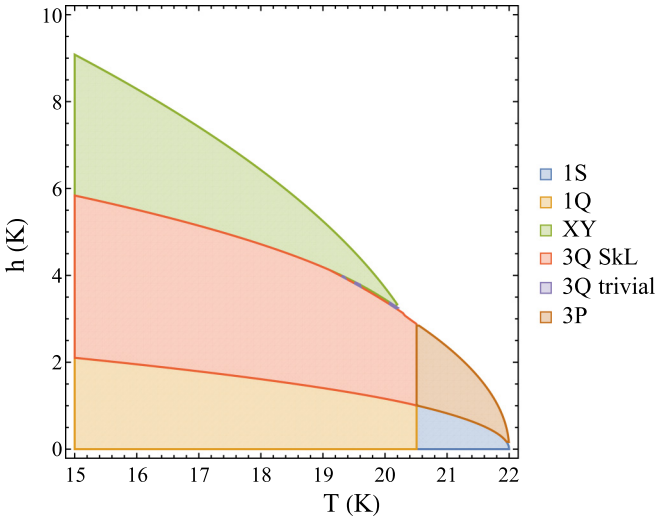

FIG. 11. If one considers standard single-ion easy-axis anisotropy without dipolar forces, the conical phase becomes stable at large fields (see text), but the skyrmion lattice is the ground state in the intermediate field range. In contrast, for easy-plane anisotropy the whole phase diagram is rather trivial, and only XY and PM phases appear.

The boundary between the $3Q$ SkL and $3Q$ trivial phases is approximately a continuation of the previous equation onto larger t:

$$t_{\mathrm{SkL}} = \frac{\Lambda}{10} + \frac{203}{45} b(\chi h)^2. \tag{35}$$

Finally, the second-order phase transition between the $3Q$ trivial phase and the PM phase takes place at

$$t_h = \Lambda_h \leftrightarrow t = \Lambda + 2b(\chi h)^2. \tag{36}$$

The equations above fix the generic type of phase diagram which can be obtained by varying the parameters of the system until the **c** axis remains the easy one for modulated spin components.

It is pertinent to make a connection with Ref. [17], which is devoted to low temperatures and considers standard easy-plane and easy-axis anisotropies. In agreement with the results of Ref. [17] we find that the phase diagram for easy-plane anisotropy is trivial and consists only of XY and PM phases. The easy-axis case is more interesting. To analyze it, we put $\Lambda = \Lambda' = 0.1$ K in parameter set (30) and observe the phase diagram shown in Fig. 11, which is similar to the one for dipolar forces and easy-axis anisotropy (see Fig. 10) but with the conical XY phase neighboring the PM phase instead of the $3Q$ trivial one. We also would like to point out that the bubble crystal ($3P$) can be stable at low temperatures if the easy-axis anisotropy is large enough [49]; in our approach it is small. Furthermore, similar to our findings, a recent paper [50] shows a temperature-induced topological transition between $3P$ and $3Q$ SkL phases at rather high temperature in the Kondo lattice model with easy-axis anisotropy.

Note that in Fig. 11, despite $\delta\Lambda = 0$, we have no traces of double-modulated phases once again. The reason for this is that in this case the XY structure has lower energy than $2S$ and $2Q$ (see Ref. [24] for details) and we are left with only a competition between XY and $3Q$ in the high-h part of the phase diagram. This resembles the results of Ref. [51], where the bimerons were shown to appear in the easy-plane case, rather than the easy-axis one.

VI. CONCLUSIONS

To conclude, we propose a simple analytical mean-field description of skyrmion lattices in hexagonal frustrated antiferromagnets capable of describing the high-temperature part of the phase diagram. We show that dipolar forces (which are always present in real compounds) are sufficient to stabilize the hexagonal SkL for the case of in-plane modulation vectors. We observe several generic types of phase diagrams and discuss the phase boundaries. One of the obtained phase diagrams can be relevant to the experimental observations in Gd_2PdSi_3 [14,43,44].

Finally, we would like to point out that a theory complementary to the one proposed here for the low-temperature part of the phase diagram is an interesting and challenging problem due to the multiharmonic skyrmion structure (see, e.g., Ref. [52]) and long-range nature of the dipolar forces. Moreover, the same problems should arise when discussing isolated skyrmions and their pairwise properties (e.g., interaction) at high temperatures, which is also an important issue.

ACKNOWLEDGMENTS

We are grateful to V. A. Ukleev for valuable discussions. This work is supported by the Russian Science Foundation (Grant No. 22-22-00028).

APPENDIX A: DIPOLAR FORCES

1. Dipolar forces as a source of momentum-dependent biaxial anisotropy

After one chooses a particular lattice geometry, all the properties of dipolar interaction in our model (2) are fixed [see also Eq. (3)]. In order to stay connected with some real compounds, we take the lattice parameters of the Gd_2PdSi_3 hexagonal lattice, $a = 4.066$ Å and $c = 4.091$ Å [35]. Nevertheless, it can be directly checked that the conclusions we made about the dipolar tensor properties are valid in a wide range of lattice parameters.

The next step in dealing with dipolar interaction is to calculate its Fourier transform. Fortunately, the appropriate technique was developed a long time ago. It is based on presenting the lattice sums in the fast-converging forms using the Poisson summation formula [46]. Nowadays, this method can be easily realized on any computer, and accurate calculations of dipolar tensor components at a certain momentum require time of the order of several seconds.

Finally, we can calculate $\mathcal{D}^{\alpha\beta}_{\mathbf{q}}$ for various $\mathbf{q}$. Let us, for example, take the $\mathbf{k}_1$ vector, for which we have $\mathcal{D}^{\alpha\beta}$ in the almost diagonal form with some numerical error (all values are in kelvins):

$$\mathcal{D}_{\mathbf{k}_1} \approx \begin{bmatrix} -0.19 & -2.3\times10^{-19} & -1.0\times10^{-37} \\ -2.3\times10^{-19} & 0.33 & 1.6\times10^{-20} \\ -1.0\times10^{-37} & 1.6\times10^{-20} & -0.15 \end{bmatrix}. \tag{A1}$$

Evidently, we have eigen-numbers of the dipolar tensor on the diagonal of this matrix. So, we have $d_1 = 0.19$ K for eigenvector $\hat{x}$, $d_2 = 0.15$ K for eigenvector $\hat{z}$, and $d_3 = -0.33$ K for eigenvector $\hat{y}$. Combined with the contribution from spherically symmetrical Heisenberg exchange (6), we arrive at three eigenvalues of $\mathcal{H}^{\alpha\beta}_{\mathbf{k}_1}$ [see Eq. (9)]: $\lambda_1(\mathbf{k}_1) = (J_{\mathbf{k}_1} + d_1)/2$, $\lambda_2(\mathbf{k}_1) = (J_{\mathbf{k}_1} + d_2)/2$, and $\lambda_3(\mathbf{k}_1) = (J_{\mathbf{k}_1} + d_3)/2$, where the biaxial anisotropy stems from the magnetodipolar interaction.

This biaxial anisotropy acts in momentum space. For example, the energy of a simple SDW with modulation vector $\mathbf{k}_1$ will depend on its polarization. The energy of this structure will be the lowest if the spins are oriented along the $\hat{x}$ direction, and the highest if the spins are oriented in the $\hat{y}$ direction (along $\mathbf{k}_1$). Moreover, components of more complicated spin structures will also feel this axis hierarchy. This allows us to say that the $\hat{x}$ direction is the easy one for structures with modulation vector $\mathbf{k}_1$, whereas the $\hat{y}$ axis is the hard one (see Fig. 2).

2. Dipolar forces and noncollinear structures' modulation vectors

In Sec. II we stated that since the dipolar interaction is much smaller than the exchange one, it is safe to assume that modulation vectors of all the modulated structures addressed in this paper are $\mathbf{k}_i$: vectors at which $J_{\mathbf{q}}$ has its maxima. Here, we show that this assumption is correct up to the first order in dipolar forces to some characteristic scale of exchange coupling ratio.

In order to show the main principle, but not fine details, we take into consideration the famous J_1-J_2 model with ferromagnetic nearest-neighbors coupling J_1 and antiferromagnetic next-nearest-neighbors coupling J_2 (bearing in mind some not-frustrated interchain coupling), which is apparently one of the simplest magnetically frustrated models. In this case, the Fourier transform of the exchange interaction reads

$$J_q = 2(J_1 \cos q - J_2 \cos 2q), \tag{A2}$$

and its maximum is given by

$$k = \arccos \frac{J_1}{4J_2}, \quad 4J_2 \geqslant J_1. \tag{A3}$$

Importantly, J_q can be expanded near its maximum as

$$J_q \approx J_k - \mathcal{J}(q-k)^2/2, \quad \mathcal{J} = \frac{(4J_2)^2 - J_1^2}{2J_2}. \tag{A4}$$

Here, parameter $\mathcal{J}$ is of the order of exchange constants.

Now we can consider a question about the SDW modulation vector in such a model with dipolar forces. It corresponds to the maximum of $\lambda_1(q)$ [eigen-number for the easy direction; see Eq. (9) and the text after it], which can be found by maximization of the equation

$$J_q + d_1(q). \tag{A5}$$

In general, the dipolar interaction contribution here can be expanded up to the linear order in $q - k$:

$$d_1(q) = d_1(k) + D(q-k), \tag{A6}$$

where constant D is of the order of $\omega_0 \ll \mathcal{J}$. Next, one can find that Eq. (A5) is maximized at $k' = k + D/\mathcal{J} \approx k$, and

$$\lambda_1(k') = \lambda_1(k) + \frac{D^2}{2\mathcal{J}} = \lambda_1(k)(1 + O[(\omega_0/\mathcal{J})^2]). \tag{A7}$$

We see that the variation of the eigen-number here is of the second order in the dipolar-to-exchange interaction ratio and can be safely neglected.

The same conclusion is evidently also true in other complicated cases: Instead of Eq. (A5) we have exchange interaction with maxima at $\mathbf{k}_i$ and some dipolar interaction contributions, which linearly alter the modulation vectors but affect eigen-numbers only in the second order. So, the assumption of using eigen-numbers and modulation vectors corresponding to maxima of the exchange interaction for the free energies of various phases (which was used everywhere in the calculations) is mathematically correct. At the same time, neglecting the modulation vectors' small variations is also safe, because it does not change the nature of the considered magnetic structures (of course, there can be some exceptions to these rules, when, for example, some commensurate phases appear due to dipolar-forces-induced anisotropy, but we do not consider them here).

APPENDIX B: FREE ENERGIES OF VARIOUS PHASES AND PHASE DIAGRAM FOR IN-PLANE EASY AXES

Here, we derive analytical expressions for the relevant phases' free energies (double-modulated phases are addressed in Ref. [24]). For magnetization components of the corresponding spin structures we use the simple approximation $m = \chi h$ with constant susceptibility parameter χ [see Eq. (23) and the discussion below]. Finally, we make conclusions about the generic phase diagram for in-plane easy axes.

1. Simple spin-density wave (1*S* phase)

In the case of the 1*S* phase there is only one component of the order parameters. It can be easily found from Eq. (13) by plugging in $m = \chi h$ and using t_h defined in Eq. (24), which yields

$$s^2 = \frac{2t_h}{3b}, \tag{B1}$$

$$\mathcal{F}_{1S} = -\frac{t_h^2}{6b} - \frac{\chi h^2}{2}, \quad t_h > 0. \tag{B2}$$

The condition $t_h = 0 \Leftrightarrow t = 2b(\chi h)^2$ determines the boundary between the 1*S* phase and the high-field paramagnetic, or induced ferromagnetic, phase (PM).

2. Single-*Q* elliptical helicoid (1*Q* phase)

The single-Q elliptical helicoid structure is characterized by two parameters, which measure the amplitude of the spin ordering along the easy and middle axes. Minimization of the free energy (15) yields

$$s^2 = \frac{2t_h + \Lambda_h}{4b}, \quad p^2 = \frac{2t_h - 3\Lambda_h}{4b} \tag{B3}$$

and

$$\mathcal{F}_{1Q} = -\frac{4t_h^2 - 4t_h\Lambda_h + 3\Lambda_h^2}{16b} - \frac{\chi h^2}{2}, \quad t_h > \frac{3}{2}\Lambda_h. \tag{B4}$$

At

$$t_h = 3\Lambda_h/2 \Leftrightarrow t_{1Q} = 3\Lambda/2 + 8b(\chi h)^2, \tag{B5}$$

continuous transition between $1S$ and $1Q$ takes place.

3. Conical helicoid (XY phase)

In the XY phase the modulated spin component rotates in the ab plane, which is perpendicular to the external field. The equations are quite similar to the $1Q$ phase ones:

$$s^2 = \frac{2t_h + \Lambda'}{4b}, \quad p^2 = \frac{2t_h - 3\Lambda'}{4b}, \tag{B6}$$

whereas the free energy reads

$$\mathcal{F}_{XY} = -\frac{4t_h^2 - 4t_h\Lambda' + 3\Lambda'^2}{16b} - \frac{\chi h^2}{2}, \quad t_h > \frac{3}{2}\Lambda'. \tag{B7}$$

The condition $t_h = \frac{3}{2}\Lambda' \Leftrightarrow t = 3\Lambda'/2 + 2b(\chi h)^2$ determines the phase boundary between the $1S$ and XY phases. Moreover, it is evident from Eqs. (B4) and (B7) that the $1Q$ and XY phases are in equilibrium when $\Lambda_h = \Lambda'$. This condition determines the so-called spiral plane flop field

$$h_{SF} = \sqrt{\frac{\Lambda' - \Lambda}{4b\chi^2}}. \tag{B8}$$

Note that at this field and $t_h = 3\Lambda_h/2 = 3\Lambda'/2$, phases $1S$, $1Q$, and XY are in equilibrium. This yields the triple-point temperature

$$t_{\mathrm{Tr}} = 2\Lambda' - \Lambda/2. \tag{B9}$$

If we for the moment forget about the $3Q$ phase, whose properties are described below, the typical phase diagram of the model (10) considered here is shown in Fig. 12, where the parameter set (30) is used. This type of phase diagram should be contrasted with those (see Figs. 6 and 7) where the $3Q$ phase is also taken into account. Note that for parameters (30) at $t \lesssim t_{\mathrm{Tr}}$, small $|\mathbf{s}_i| \ll S$ expansion is inapplicable: Using Eq. (B1), one obtains $s \approx 2.5$ for $t = t_{\mathrm{Tr}}$ and $h = h_{SF}$.

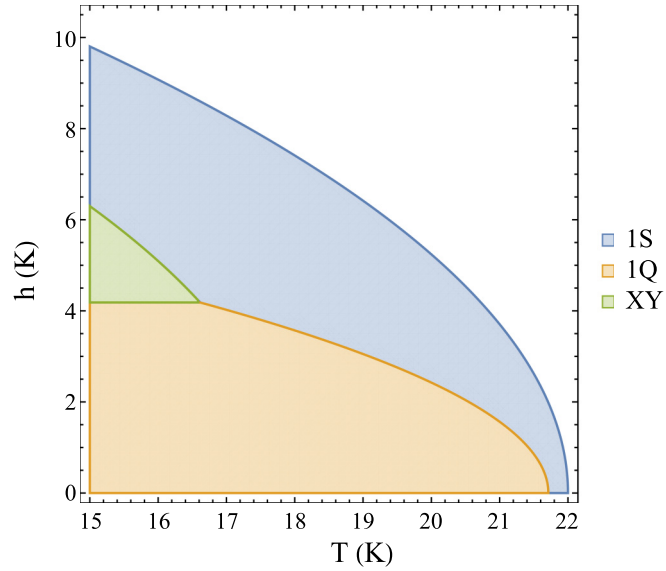

FIG. 12. High-temperature part of the phase diagram for the considered model with in-plane easy axes, where (for illustration purposes) the $3Q$ phase was excluded from the analysis. Parameters (30) were used.

4. Superposition of three screw helicoids ($3Q$ phase)

In the case of the $3Q$ phase the free energy is a function of three s_j, three p_j, and three phases φ_j [see Eq. (18)]. The general expression for it is quite cumbersome; to make it shorter, we introduce $s_\Sigma^2 = s_1^2 + s_2^2 + s_3^2$, $p_\Sigma^2 = p_1^2 + p_2^2 + p_3^2$. As a result we get

$$\begin{aligned}\mathcal{F}_{3Q} = -\frac{t}{2}s_\Sigma^2 - \frac{t-\Lambda}{2}p_\Sigma^2 - hm - (t-\Lambda_0)m^2 + b\Bigg[m^4 + m^2\left(s_\Sigma^2 + 3p_\Sigma^2\right) + \frac{3\left(s_\Sigma^2\right)^2 + 2s_\Sigma^2 p_\Sigma^2 + 3\left(p_\Sigma^2\right)^2}{8} \\ + \frac{3\left(p_1^2p_2^2 + p_1^2p_3^2 + p_2^2p_3^2\right)}{4} + \frac{s_1^2\left(p_2^2 + p_3^2\right) + s_2^2\left(p_1^2 + p_3^2\right) + s_3^2\left(p_1^2 + p_2^2\right)}{4} \\ - m(6p_1p_2p_3 + s_1s_2p_3 + s_1s_3p_2 + s_2s_3p_1)\sin(\varphi_1 + \varphi_2 + \varphi_3)\Bigg].\end{aligned} \tag{B10}$$

Importantly, the first line here constitutes the free energy of the $1Q$ phase if one puts $s_\Sigma = s$, $p_\Sigma = p$ [cf. Eq. (15)], whereas the second and the third lines determine the "penalty" and the "profit" for having $3Q$ structure instead of $1Q$, respectively. They can be considered as effective "cubic anisotropy" in the order parameter space. Evidently, the superposition of two helicoids has no advantages in this model, because the last term in Eq. (B10) is zero. So, we are left with two possibilities: One can have a single helicoid component (e.g., with nonzero s_1 and/or p_1), or all three helicoids. In the former case we arrive at the free energy given by Eq. (15), while in the latter case it can be checked that the minimum of the free energy corresponds to the spin structure (18) with all equal s_i and p_i, and $\sum_i \varphi_i = \pi/2 + \pi n$ with integer n (the signs of s and p should be properly chosen). This leads to the free energy of the $3Q$ phase in the form of Eq. (20).

Analytical minimization of the free energy (20) (using the trick with magnetization described above) leads to a system of

cubic equations:

$$-t_h s + b\left(\frac{3}{2}s^3 + \frac{5}{6}sp^2 - \frac{2\chi hsp}{\sqrt{3}}\right) = 0,$$
$$-(t_h - \Lambda_h)p + b\left(\frac{5}{2}p^3 + \frac{5}{6}s^2 p - \frac{\chi h(s^2+6p^2)}{\sqrt{3}}\right) = 0. \tag{B11}$$

The first one gives either $s = 0$ or

$$s^2 = \frac{2}{3}\left(\frac{t_h}{b} - \frac{5}{6}p^2 + \frac{2\chi hp}{\sqrt{3}}\right), \tag{B12}$$

which can be plugged into the second equation in the system (B11). After some algebra, we arrive at the following cubic equation for p:

$$p^3 - \frac{39\sqrt{3}\chi h}{55}p^2 + \left[\frac{24}{11}(\chi h)^2 + \frac{27}{55b}\left(\Lambda - \frac{4}{9}t\right)\right]p - \frac{6\sqrt{3}\chi h t_h}{55b} = 0. \tag{B13}$$

This equation can be solved using Cardano's formula. To make the corresponding result more compact, first we introduce

$$\alpha = \frac{39\sqrt{3}\chi h}{55}, \quad \beta = \frac{24}{11}(\chi h)^2 + \frac{27}{55b}\left(\Lambda - \frac{4}{9}t\right),$$
$$\gamma = \frac{6\sqrt{3}\chi h t_h}{55b}, \quad \rho = \alpha^2 - 3\beta, \quad \sigma = 2\alpha^3 - 9\alpha\beta + 27\gamma. \tag{B14}$$

Using these expressions, we can write solutions for p in the form

$$p = \frac{\alpha}{3} - \frac{(-1)^{1/3}2^{1/3}\rho}{3(\sigma + \sqrt{\sigma^2 - 4\rho^3})^{1/3}} - \frac{(\sigma + \sqrt{\sigma^2 - 4\rho^3})^{1/3}}{(-1)^{1/3}2^{1/3}3}, \tag{B15}$$

where $(-1)^{1/3} = -1, (1 + i\sqrt{3})/2, (1 - i\sqrt{3})/2$; these values should be plugged simultaneously into both the second and the third terms of Eq. (B15), whereas the other cube roots should be taken for the branch $(-1)^{1/3} = -1$.

The $3Q$ phase is (meta)stable at $t > 2b(\chi h)^2$, where there is an instability towards nonzero s value, which, in its turn, leads to nonzero p in the external field due to the term $\propto mps^2$ [see Eq. (20)]. Analysis shows that in this region of the phase diagram, the proper solution for p is given by Eq. (B15) with $(-1)^{1/3} = -1$. Then, one can calculate s using Eq. (B12). Finally, plugging these particular p and s into Eq. (20) with $m = \chi h$, one could obtain an analytical expression for the $3Q$ phase free energy. We will not write down it here explicitly, because it is cumbersome.

5. Double-modulated spin structures ($2S$ and $2Q$)

The double-modulated spin structures' free energies in the developed framework are addressed in detail in Ref. [24]. Here, we just describe necessary changes, when there is $\delta\Lambda > 0$ (see Sec. III).

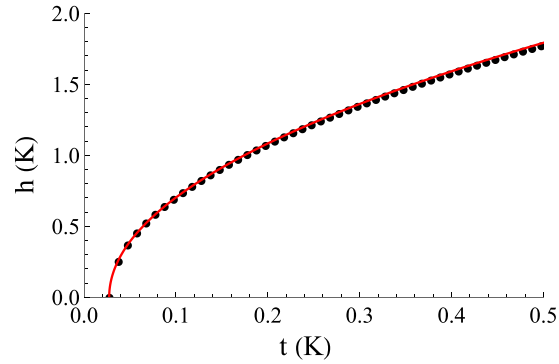

FIG. 13. Illustration of empirical law (B18) for the boundary between the $1Q$ and $3Q$ phases. Black dots stand for the numerical solution of the $\mathcal{F}_{1Q} = \mathcal{F}_{3Q}$ equation, whereas the red line is for Eq. (B18). Parameter set (30) is used.

Using Eq. (22), one can easily obtain

$$\mathcal{F}_{2S} = -\frac{(t_h - \delta\Lambda)^2}{5b} - \frac{\chi h^2}{2}, \quad t_h > \delta\Lambda, \tag{B16}$$

for the vortical $2S$ phase. At $t_h - \delta\Lambda > 5(\Lambda_h - \delta\Lambda)/2$ it continuously transforms into a $2Q$ structure with the free energy

$$\mathcal{F}_{2Q} = -\frac{8(t-\delta\Lambda)^2 - 4(t-\delta\Lambda)(\Lambda - \delta\Lambda) + 5(\Lambda - \delta\Lambda)^2}{36b} - \frac{\chi h^2}{2}, \quad t_h > \delta\Lambda + 5(\Lambda_h - \delta\Lambda)/2. \tag{B17}$$

6. Phase boundaries

After free-energy derivation, we can turn to analysis of the boundary between the $1Q$ and $3Q$ phases. An approximate expression for this curve was obtained by fitting numerical data for various parameter sets. The result is the following:

$$t_{1Q-3Q}(h) \approx \tfrac{3}{2}\Lambda + 45b(\chi h)^2. \tag{B18}$$

This expression works quite well for not very small h, where the linear-in-h term is somewhat important. Particular usage of this expression for parameter set (30) is shown in Fig. 13. Note that at given h, Eq. (B18) yields a much larger temperature than Eq. (B5). For instance, at h_{SF} [see Eq. (B8)] one has $t_{1Q-3Q} \approx 3\Lambda/2 + 11.25(\Lambda' - \Lambda)$, which is a very large quantity for our approach [note that for parameter set (30) it corresponds to $T < 0$]. Nevertheless, it shows that the $3Q$ phase should be stable even at temperatures substantially lower than the ordering one (T_c). This can also be illustrated by manually making Λ' in parameter set (30) be much smaller than 0.26 K, e.g., equal to 0.05 K. Then, the XY phase appears at larger temperatures, and its traces become visible in the phase diagram; see Fig. 7.

Topological properties of the $3Q$ phase depend on whether the spins can wrap around the whole sphere in the spin space or not. In the external field along the **c** axis, this requires that the maximal negative value of the modulated z component of spin (which is equal to $-3p/\sqrt{3}$) overcomes positive magnetization m. So, the boundary between the $3Q$ trivial and $3Q$ SkL phases is given by the equation $p = m/\sqrt{3}$. We plug this into Eq. (B13). Then, it can be shown that this equation is satisfied

if

$$t = t_{\mathrm{SkL}} = \tfrac{9}{10}\Lambda + \tfrac{203}{45} b(\chi h)^2 \approx 0.9\Lambda + 4.5b(\chi h)^2. \tag{B19}$$

At larger t (smaller temperatures T) the structure is topologically nontrivial with $n_{Sk} = \pm 1$ (depending on the choice of the three constituent helicoids' chiralities) per magnetic unit cell.

Finally, by comparing the free energy of the $1Q$ phase (B4) and that of the $2Q$ phase (B17) we can find a condition under which double-modulated phases can be visible in the phase diagram as, e.g., in Fig. 8. The physical solution of equation $\mathcal{F}_{1Q} = \mathcal{F}_{2Q}$ reads

$$t_h = \tfrac{1}{2}\big(-12\delta\Lambda + 5\Lambda_h + 3\sqrt{2}\sqrt{10\delta\Lambda^2 - 8\Lambda_h\delta\Lambda + \Lambda_h^2}\big), \tag{B20}$$

which should be larger than $\delta\Lambda + 5(\Lambda_h - \delta\Lambda)/2$. The last condition at $h = 0$ yields

$$\delta\Lambda < \frac{8 - \sqrt{42}}{11}\Lambda \approx 0.14\Lambda. \tag{B21}$$

This is the precise formulation of the condition $\delta\Lambda \ll \Lambda$, which was used in Secs. III and IV.

APPENDIX C: FREE ENERGIES OF VARIOUS PHASES AND PHASE DIAGRAM FOR OUT-OF-PLANE COLLINEAR EASY AXES

When the easy axes for possible modulation vectors $\mathbf{k}_j$ are collinear and oriented along the $\mathbf{c}$ axis, the formulas are similar to those of Appendix B; however, some important differences appear. Here, we discuss them in detail and obtain the corresponding phase boundaries.

In the external magnetic field it is convenient to use the renormalized parameters given by Eqs. (31) and (32) [cf. Eqs. (24) and (25)].

1. Simple spin-density wave ($1S$ phase)

In the $1S$ phase the spin polarization is along the easy axis $\mathbf{c}$, so it is parallel to the magnetic field:

$$\mathbf{s}_i = (s\cos\mathbf{k}_1\mathbf{R}_i + m)\hat{z}. \tag{C1}$$

For s and $\mathcal{F}_{1S}$ one should use Eqs. (B1) and (B2), but with t_h defined in Eq. (31). The boundary between PM and $1S$ is thus defined by the condition

$$t_h = 0 \Leftrightarrow t = 6b(\chi h)^2. \tag{C2}$$

2. Single-Q elliptical helicoid ($1Q$ phase)

We left the definition of the single-Q elliptical helicoid spin ordering (14) intact, so in comparison with Eqs. (B3) the spin components should be interchanged:

$$p^2 = \frac{2t_h + \Lambda_h}{4b}, \quad s^2 = \frac{2t_h - 3\Lambda_h}{4b}, \tag{C3}$$

where conditions $t_h > 3\Lambda_h/2$ and $t_h > -\Lambda_h/2$ should hold (the last one can be violated in the external field). Importantly, the former one defines the boundary between the $1S$ and $1Q$ phases, which is a simple vertical line:

$$t_h = 3\Lambda_h/2 \Leftrightarrow t = 3\Lambda/2. \tag{C4}$$

The free energy of $1Q$ is given exactly by Eq. (B4).

3. Conical helicoid (XY phase)

The modulated components of spins in the conical phase are rotating in the hard plane. As compared with the previous $1Q$ case, substitutions $t_h \to t_h' - \Lambda$ and $\Lambda_h \to \Lambda' - \Lambda$ are in order, where $t_h' = t - 2b(\chi h)^2$. So, the XY phase free energy reads

$$\mathcal{F}_{XY} = -\frac{4(t_h' - \Lambda)^2 - 4(t_h' - \Lambda)(\Lambda' - \Lambda) + 3(\Lambda' - \Lambda)^2}{16b} - \frac{\chi h^2}{2}, \quad t_h' > \frac{3\Lambda' - \Lambda}{2}. \tag{C5}$$

Importantly, the spiral plane flop field in this case reads

$$h_{SF} = \sqrt{\frac{\Lambda'}{4b\chi^2}}, \tag{C6}$$

which is larger than the one for the in-plane easy-axes case [see Eq. (B8)].

4. Superposition of three screw helicoids ($3Q$ phase)

For the $3Q$ phase, one should make the following substitution in the free energy (B10):

$$-\frac{t}{2}s_\Sigma^2 - \frac{t-\Lambda}{2}p_\Sigma^2 \longrightarrow -\frac{t}{2}p_\Sigma^2 - \frac{t-\Lambda}{2}s_\Sigma^2, \tag{C7}$$

which leads to qualitatively new behavior of order parameters in comparison with the case of in-plane easy axes.

The counterparts of Eqs. (B11) read

$$-(t_h - \Lambda_h)s + b\left(\frac{3}{2}s^3 + \frac{5}{6}sp^2 - \frac{2\chi hsp}{\sqrt{3}}\right) = 0,$$
$$-t_h p + b\left(\frac{5}{2}p^3 + \frac{5}{6}s^2 p - \frac{\chi h(s^2 + 6p^2)}{\sqrt{3}}\right) = 0. \tag{C8}$$

We can rewrite the first equation as

$$s\left[\frac{3}{2}bs^2 + \frac{5b}{6}p^2 - \frac{2b\chi hp}{\sqrt{3}} - (t_h - \Lambda_h)\right] = 0. \tag{C9}$$

Assuming $s = 0$ in the second equation of the system (C8), and plugging its p-dependent part into Eq. (C9), we find that there are no additional solutions for s if $t_h \leqslant 3\Lambda_h/2 \Leftrightarrow t \leqslant 3\Lambda/2$. Then, we arrive at an interesting conclusion: In this region of parameters the $3Q$ phase is just a superposition of three collinear SDWs. We will refer to this spin structure as $3P$. It is illustrated in Fig. 9. Evidently, this phase is topologically trivial. The corresponding order parameter p can be simply obtained from the quadratic equation, the result being

$$p = \tfrac{1}{5}(2\sqrt{3}\chi h + \sqrt{12(\chi h)^2 + 10t_h/b}). \tag{C10}$$

Together with $s = 0$ and $m = \chi h$ it allows us to calculate the $3P$ phase free energy.

For $t > 3\Lambda/2$, parameter s is nonzero, and (as in Appendix B) one needs to solve the cubic equation:

$$p^3 - \frac{39\sqrt{3}\chi h}{55}p^2 + \left[\frac{24}{11}(\chi h)^2 - \frac{3}{55b}(4t+5\Lambda)\right]p - \frac{6\sqrt{3}\chi h(t_h-\Lambda_h)}{55b} = 0. \quad \text{(C11)}$$

In order to utilize solutions (B15), one should use modified parameters

$$\beta = \frac{24}{11}(\chi h)^2 - \frac{3}{55b}(4t+5\Lambda), \quad \gamma = \frac{6\sqrt{3}\chi h(t_h-\Lambda_h)}{55b}, \quad \text{(C12)}$$

along with α, σ, and ρ from Eqs. (B14).

5. Phase boundaries

We start from the phase boundaries at $t \leqslant 3\Lambda/2$. In this region, the competing phases are PM, $1S$, and $3P$. By comparing the free energies, we find that there is a boundary between $1S$ and $3P$ which reads

$$t_{1S-3P} = \left[\frac{\sqrt{6}-1}{(\sqrt{6}-2)^2}\frac{24}{5} + 6\right]b(\chi h)^2 \approx 40b(\chi h)^2. \quad \text{(C13)}$$

At given t the $1S$ phase is stable below this curve (at smaller fields) in the T-H plane, and $3P$ is stable above it.

At yet higher magnetic fields, there is a first-order transition between $3P$ and PM, which is evident from the $3P$ phase free energy (bearing in mind that $s = 0$ and $m = \chi h$), which has the form [cf. Eq. (20)]

$$\mathcal{F}_{3P} = -\frac{t_h}{2}p^2 - \frac{\chi}{2}h^2 + b\left[\frac{5p^4}{8} - \frac{2\chi h p^3}{\sqrt{3}}\right]. \quad \text{(C14)}$$

The cubic term here induces discontinuous transition. After some algebra we find the phase boundary

$$t_{3P-\mathrm{PM}} = \tfrac{74}{15}b(\chi h)^2. \quad \text{(C15)}$$

Note that $t_{3P-\mathrm{PM}}$ is always smaller than the t_{1S-3P} at given h, so there is no boundary between the $1S$ and PM phases.

At $t > 3\Lambda/2$, nonzero s appears. So, $1Q$, $3Q$, and PM are competing. The boundary between $1Q$ and $3Q$ is hard to find explicitly; however, we observe that Eq. (C13) describes this curve quite accurately. In the high-fields domain the transition between $3Q$ SkL and PM can be either direct (the first-order one) or via the intermediate $3Q$ trivial phase. This should be contrasted with the in-plane easy-axes case, where the $3Q$ trivial phase always appears before the PM phase. The $3Q$ trivial phase continuously transforms into PM at

$$t_h = \Lambda_h \leftrightarrow t = \Lambda + 2b(\chi h)^2. \quad \text{(C16)}$$

Moreover, the boundary (if it exists) between the $3Q$ SkL and $3Q$ trivial phases can be found analytically from the condition $p = m/\sqrt{3}$. Plugging the latter into the cubic equation (C11), we can find the corresponding curve

$$t_{\mathrm{SkL}} = \frac{\Lambda}{10} + \frac{203}{45}b(\chi h)^2. \quad \text{(C17)}$$

Importantly, curves (C16) and (C17) intersect at $t' = 194\Lambda/113 \approx 1.72\Lambda$, which is larger than $3\Lambda/2$. This means that below t' the $3Q$ trivial phase does not exist. In the range $t \in (1.5\Lambda, 1.72\Lambda)$ there is a first-order transition between the $3Q$ SkL and PM phases. The boundary between them interpolates the two curves (C15) and (C17). At $t > t'$ the line of the first-order transitions (here, between the $3Q$ SkL and $3Q$ trivial phases) is approximately given by Eq. (C17). It terminates at $t = t''$ (it will be quantified below). In the region of temperatures $t' < t < t''$ at relevant magnetic fields, t_{SkL} corresponds to the spurious real solution for p, whereas the physical solution discontinuously jumps from $p > m/\sqrt{3}$ to $p < m/\sqrt{3}$. At $t > t''$ there is only one physical solution, which continuously changes with h, and there is a smooth crossover between the $3Q$ SkL and $3Q$ trivial phases at t_{SkL} given by Eq. (C17).

Finally, we discuss the analytical derivation of t''. At this temperature the plot for $p(h)$ has a vertical tangent; at $t < t''$ there is a region of fields with three real solutions, and at $t > t''$ there is only one real solution in the high-fields domain (near the PM phase stability part of the phase diagram). In order to obtain t'', we rewrite Eq. (C11) in the form

$$p^3 - \frac{39\sqrt{3}\chi h}{55}p^2 + \left[\frac{24}{11}(\chi h)^2 - \frac{3}{55b}(4t+5\Lambda)\right]p = \frac{6\sqrt{3}\chi h(t_h-\Lambda_h)}{55b}, \quad \text{(C18)}$$

where the right-hand side is p independent. Then, the solutions can be found graphically, as intersections of cubic parabola and the horizontal line. At t'' the left-hand side (l.h.s.) should have a horizontal tangent and inflection at the same point. So, conditions $\partial\text{l.h.s.}/\partial p = 0$ and $\partial^2\text{l.h.s.}/\partial p^2 = 0$ should hold simultaneously with Eq. (C18). The latter simply yields $p = 13\sqrt{3}\chi h/55$; plugging it into the former, we get $4t'' + 5\Lambda = 1693b(\chi h)^2/55$. Next, using these two formulas and Eq. (C18), we obtain

$$t'' = \frac{2\times 93\,115 + 5\times 14\,297}{2\times 93\,115 - 4\times 14\,297}\Lambda \approx 2\Lambda. \quad \text{(C19)}$$

Note that $t'' > t' > 1.5\Lambda$, so the above-discussed topology of the phase diagram should be independent of the parameters of a model, until the easy axes are collinear.

[1] A. N. Bogdanov and C. Panagopoulos, Nat. Rev. Phys. **2**, 492 (2020).

[2] B. Göbel, I. Mertig, and O. A. Tretiakov, Phys. Rep. **895**, 1 (2021).

[3] A. N. Bogdanov and D. Yablonskii, Sov. Phys. JETP **68**, 101 (1989).

[4] A. Bogdanov and A. Hubert, J. Magn. Magn. Mater. **138**, 255 (1994).

[5] S. Mühlbauer, B. Binz, F. Jonietz, C. Pfleiderer, A. Rosch, A. Neubauer, R. Georgii, and P. Böni, Science **323**, 915 (2009).

[6] A. Fert, V. Cros, and J. Sampaio, Nat. Nanotechnol. **8**, 152 (2013).

[7] A. Fert, N. Reyren, and V. Cros, Nat. Rev. Mater. **2**, 17031 (2017).

[8] A. A. Belavin and A. M. Polyakov, JETP Lett. **22**, 245 (1975).

[9] A. Neubauer, C. Pfleiderer, B. Binz, A. Rosch, R. Ritz, P. G. Niklowitz, and P. Böni, Phys. Rev. Lett. **102**, 186602 (2009).

[10] I. Dzyaloshinsky, J. Phys. Chem. Solids **4**, 241 (1958).

[11] T. Moriya, Phys. Rev. **120**, 91 (1960).

[12] T. Kurumaji, Phys. Sci. Rev. **5**, 20190016 (2020), and references therein..

[13] M. Kakihana, D. Aoki, A. Nakamura, F. Honda, M. Nakashima, Y. Amako, T. Takeuchi, H. Harima, M. Hedo, T. Nakama, and Y. Ōnuki, J. Phys. Soc. Jpn. **88**, 094705 (2019).

[14] T. Kurumaji, T. Nakajima, M. Hirschberger, A. Kikkawa, Y. Yamasaki, H. Sagayama, H. Nakao, Y. Taguchi, T.-h. Arima, and Y. Tokura, Science **365**, 914 (2019).

[15] T. T. J. Mutter, A. O. Leonov, and K. Inoue, Phys. Rev. B **100**, 060407(R) (2019).

[16] T. Okubo, S. Chung, and H. Kawamura, Phys. Rev. Lett. **108**, 017206 (2012).

[17] A. Leonov and M. Mostovoy, Nat. Commun. **6**, 8275 (2015).

[18] S.-Z. Lin and S. Hayami, Phys. Rev. B **93**, 064430 (2016).

[19] S. Hayami, J. Magn. Magn. Mater. **513**, 167181 (2020).

[20] S. Hayami and Y. Motome, Phys. Rev. B **103**, 054422 (2021).

[21] N. D. Khanh, T. Nakajima, X. Yu, S. Gao, K. Shibata, M. Hirschberger, Y. Yamasaki, H. Sagayama, H. Nakao, L. Peng, K. Nakajima, R. Takagi, T.-h. Arima, Y. Tokura, and S. Seki, Nat. Nanotechnol. **15**, 444 (2020).

[22] S. Hayami and Y. Motome, Phys. Rev. B **103**, 024439 (2021).

[23] Z. Wang, Y. Su, S.-Z. Lin, and C. D. Batista, Phys. Rev. B **103**, 104408 (2021).

[24] O. I. Utesov, Phys. Rev. B **103**, 064414 (2021).

[25] H. Shiba, Solid State Commun. **41**, 511 (1982).

[26] R. Gekht, Zh. Eksp. Teor. Fiz. **87**, 2095 (1984) [Sov. Phys. JETP **60**, 1210 (1984)].

[27] R. S. Gekht, Sov. Phys.-Usp. **32**, 871 (1989), and references therein.

[28] T. Sato, H. Kadowaki, H. Masudo, and K. Iio, J. Phys. Soc. Jpn. **63**, 4583 (1994).

[29] T. Sato, H. Kadowaki, and K. Iio, Phys. B: Condens. Matter **213–214**, 224 (1995).

[30] O. I. Utesov and A. V. Syromyatnikov, Phys. Rev. B **95**, 214420 (2017).

[31] O. Utesov and A. Syromyatnikov, J. Magn. Magn. Mater. **475**, 98 (2019).

[32] O. Utesov and A. Syromyatnikov, J. Magn. Magn. Mater. **527**, 167732 (2021).

[33] P. Kotsanidis, J. Yakinthos, and E. Gamari-Seale, J. Magn. Magn. Mater. **87**, 199 (1990).

[34] R. White, *Quantum Theory of Magnetism*, Springer Series in Solid-State Sciences (Springer-Verlag, Berlin, 1983).

[35] F. Tang, M. Frontzek, J. Dshemuchadse, T. Leisegang, M. Zschornak, R. Mietrach, J.-U. Hoffmann, W. Löser, S. Gemming, D. C. Meyer, and M. Loewenhaupt, Phys. Rev. B **84**, 104105 (2011).

[36] S. Banerjee, O. Erten, and M. Randeria, Nat. Phys. **9**, 626 (2013).

[37] J. Chen, D.-W. Zhang, and J.-M. Liu, Sci. Rep. **6**, 29126 (2016).

[38] A. I. Akhiezer, S. Peletminskii, and V. G. Baryakhtar, *Spin Waves* (North-Holland, New York, 1968).

[39] Except for the $1Q$ structure, which can be also described by Eq. (18).

[40] This degeneracy can be lifted by taking into account $\propto s^6$ terms in the free energy. The result is that the $1S$ free energy is always slightly smaller than the $3S$ one.

[41] U. K. Roessler, A. Bogdanov, and C. Pfleiderer, Nature (London) **442**, 797 (2006).

[42] A. O. Leonov and A. N. Bogdanov, New J. Phys. **20**, 043017 (2018).

[43] M. Hirschberger, T. Nakajima, M. Kriener, T. Kurumaji, L. Spitz, S. Gao, A. Kikkawa, Y. Yamasaki, H. Sagayama, H. Nakao, S. Ohira-Kawamura, Y. Taguchi, T.-h. Arima, and Y. Tokura, Phys. Rev. B **101**, 220401(R) (2020).

[44] S. Spachmann, A. Elghandour, M. Frontzek, W. Löser, and R. Klingeler, Phys. Rev. B **103**, 184424 (2021).

[45] T. Nagamiya, K. Nagata, and Y. Kitano, Prog. Theor. Phys. **27**, 1253 (1962).

[46] M. H. Cohen and F. Keffer, Phys. Rev. **99**, 1128 (1955), and references therein.

[47] S. Hayami and R. Yambe, Phys. Rev. B **104**, 094425 (2021).

[48] The corresponding spin structure is given by Eq. (18) with all $s_j = 0$, $p_1 = p_2 = p_3 = p/\sqrt{3}$, and $\varphi_1 + \varphi_2 + \varphi_3 = 2\pi n + \mathrm{sgn}(p)\pi/2$.

[49] S. Hayami, S.-Z. Lin, and C. D. Batista, Phys. Rev. B **93**, 184413 (2016).

[50] S. Hayami, New J. Phys. **23**, 113032 (2021).

[51] Y. A. Kharkov, O. P. Sushkov, and M. Mostovoy, Phys. Rev. Lett. **119**, 207201 (2017).

[52] V. E. Timofeev, A. O. Sorokin, and D. N. Aristov, Phys. Rev. B **103**, 094402 (2021).